ARMA 12-179

Modeling mixed-mode fracture propagation in 3D

Meng, C. and Pollard, D. D.

Department of Geological and Environmental Sciences, Stanford University, Stanford, CA 94305-2115 USA.

This paper was prepared for presentation at the 46th US Rock Mechanics / Geomechanics Symposium held in Chicago, IL, USA, 24-27 June 2012.

ABSTRACT: A planar fracture when subjected to sufficient tensile and shear stresses will propagate off-plane, known as mixed-mode propagation. Predicting the fracture path relies on the propagation criteria. The criterion we present scales the propagation magnitude and direction with the near-tip tensile stress in form of vectors that originate from the fracture tip-line. Boundary element method (BEM) enables us to calculate the near-tip stress field of an arbitrary fracture. We feed the near-tip stress to the propagation criterion to determine the propagation vectors. We grow the BEM mesh by adding new tip-elements whose size and orientation are given by the propagation vectors. Then, we feed the new mesh back to BEM to calculate the new near-tip stress. By running BEM and the propagation criterion in a loop, we are able to model 3D fracture propagation. We use analytical Eshelby's solution that evaluates near-tip stress of an ellipsoidal fracture to validate the BEM results.

1. INTRODUCTION

A planar rock fracture under sufficient mixed-mode loading will develop into off-plane geometries, [1], [2], [3], [4] and [5]. Modeling such propagation poses great challenges because of the tip-line three dimensionality and resulting complex near-tip stress field.

Under mode I II loading, i.e. normal opening and shear in the direction of the tip-line advancing, the fracture front will *kink* from its initial propagation trajectory accommodating the local stress field, Figure 1**A**. If the shear is planar, the kink angle is then uniform and the tip-line integrity is preserved. Such kinked propagation can be modeled in 2D. [6], [7] and [8] determined the off-plane growth by linear elastic fracture mechanics (LEFM) theory. [9] and [10] used 2D Displacement Discontinuity Method (DDM) to model mode I II fracture propagation.

Under mode I III loading, i.e. normal opening and shear parallel to the tip-line, the fracture front will twist as in Fig. 1B and break into segments, [11]. Such off-plane growth has to be modeled in 3D. [5] modeled the twisted (echelon shaped) fracture propagation using a 3D phase field method where the surrounding media of the fracture had to be meshed. [12] modeled mixed mode fatigue crack growth using boundary element method (BEM), where only the fracture, as 3D surface, was meshed. However [12] did not allow the fracture tip-line to break into segment, so the complete mode III effect was not captured.

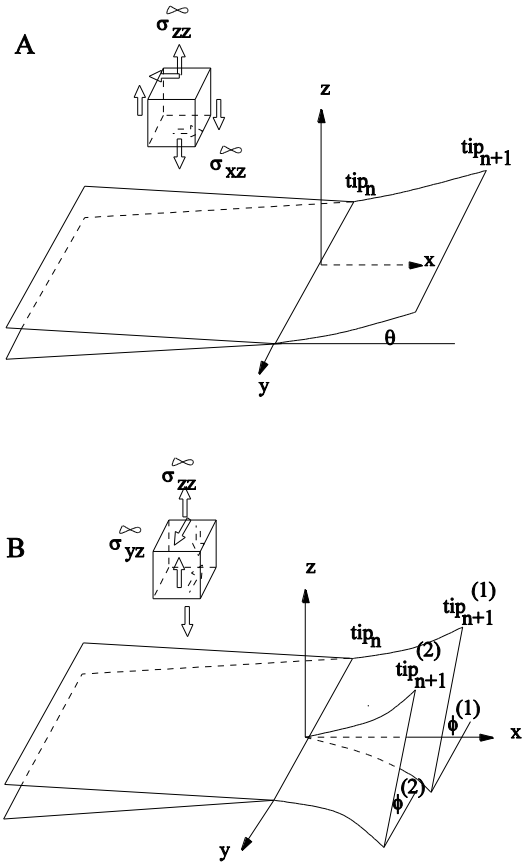

Figure 1 A, a mixed mode I II fracture starts to kink with angle θ at *n*th step of propagation; **B**, a mixed mode I III fracture starts to twist and segment with angle $\varphi^{(i)}$ at *n*th step of propagation.

The numerical scheme we present handles both kinked and twisted (segmented) fracture growth with a unified

approach. The numerical method used to compute the stress field in the vicinity of a fracture is 3D BEM, [13] and [14], based on angular dislocations, [15] and [16]. To validate the BEM results, we compare them to Eshelby's solution, [17], [18] and [19], that analytically evaluates stress fields about an ellipsoidal fracture, [20] and [21]. Using the near-tip stresses as inputs, we apply fracture propagation criterion, [3] and [5], to predict the fracture front growth.

The modeled fracture propagates by adding new elements to the exiting fracture front [12]. Different than [12], we allow the tip-line to break into segments while twisting, which forms the echelon shaped new fracture tip.

2. NEAR-TIP STRESS EVALUATION: BEM VALIDATION USING ESHELBY'S SOLUTION

Boundary element method is implemented using the commercial software iBEM, formally known as Poly3D, [13] and [14]. iBEM solves for the displacement on each of the fracture faces and calculates the associated elastic fields (stress, strain and displacement) on some given observation grids.

Eshelby's solution is implemented using a Matlab™ code by [21]. Like the BEM it computes the elastic fields on given observation grids. We use a highly eccentric ellipsoid to emulate the flat geometry of an elliptical fracture. To compare the results, the BEM meshes the same ellipse.

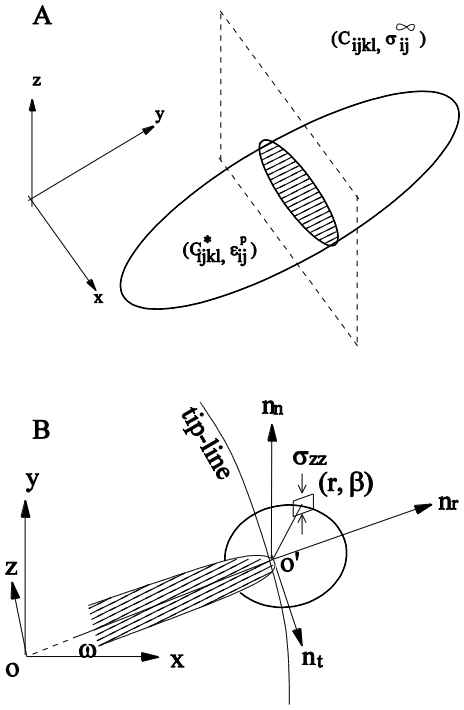

Figure 2 A, An observation grid (dashed rectangle) cutting an ellipsoidal fracture on a cross-section (shadowed). **B**, a fracture cross-section (shadowed) with longitude angel ω and polar coordinates (r,β) around the fracture tip at o',

2.1 Mode I near-tip stress comparisons

To compare the stress fields, we make cross-sectional observation grids cutting the fracture profile, Figure 2**A**. To compare the stress concentrations approaching the tip, we make circular observation grids around the tip, Figure 2**B**.

For an elliptical fracture $a_y/a_x=0.5$, we set a uni-axial tensile stress, $\sigma_{zz}^{\infty}>0$ and $\eta=0$ in Figure 3. The fracture is then under pure mode I loading.

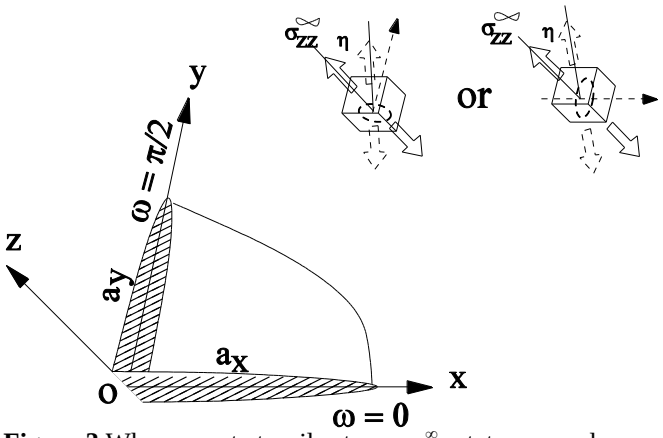

Figure 3 When remote tensile stress σ_{zz}^{∞} rotates around *y* axis, the tip at $\omega=0$ is in mixed mode I II; when stress σ_{zz}^{∞} rotates around *x* axis by angle η, the tip at $\omega=0$ is in mode I III.

We compare the normalized maximum tensile stress $\sigma_3/\sigma_3^{\infty}$ produced by the BEM and Eshelby's solution on the cross-section slice (*x-o-z* plane) that cuts the elliptical fracture in the middle. The comparison is given in Figure 4.

The comparison shows that BEM and Eshelby's solution agree well. The stress concentrates near the fracture tips and reduces to zero on the fracture faces.

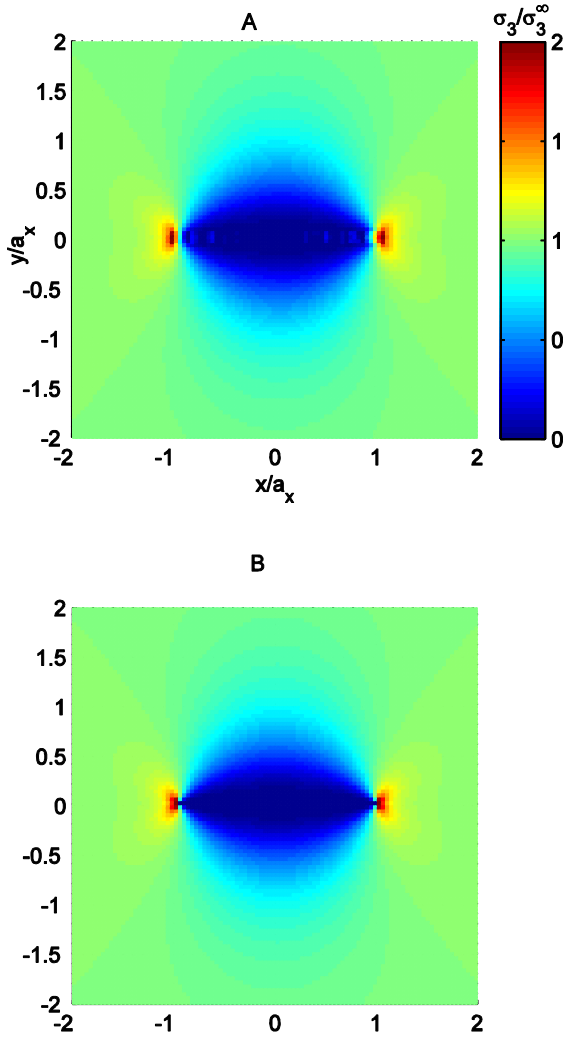

Figure 4 Normalized maximum tensile stress by BEM (**A**) and by Eshelby's solution (**B**) under pure normal stress σ_{zz}^{∞} plotted on *x*-*o*-*z* plane.

To compare the near-tip stress distributions, we zoom in about the fracture tip at longitude ω=0, i.e. $x=a_x$, $y=z=0$. The comparison is given in Figure 5.

The BEM produces higher near-tip stress than does Eshelby's solution. Indeed, the angular dislocations [15] employed by BEM produces stress singularity of order *1/r*, whereas, due to the blunt tip of the ellipsoid, Eshelby's solution results in a finite stress at $r=0$.

Validations of Eshelby's solution can be found in [21] where the ellipsoid are transformed into some less general geometries, e.g. elliptical cylinder, for which solutions are known, e.g. by [22].

Note, the theory of linear elastic fracture mechanics (LEFM) has near-tip stress singularity in order of $1/\sqrt{r}$, which is in between BEM and Eshebly's solution.

The BEM result has some scattered non-zero stress on the fracture faces behind the tip ($x<a_x$, $y=z=0$), whereas Eshelby's solution has zero stress on the faces.

The face boundary condition of the BEM model is set as traction free. However, this is not strictly honored due to some numerical errors.

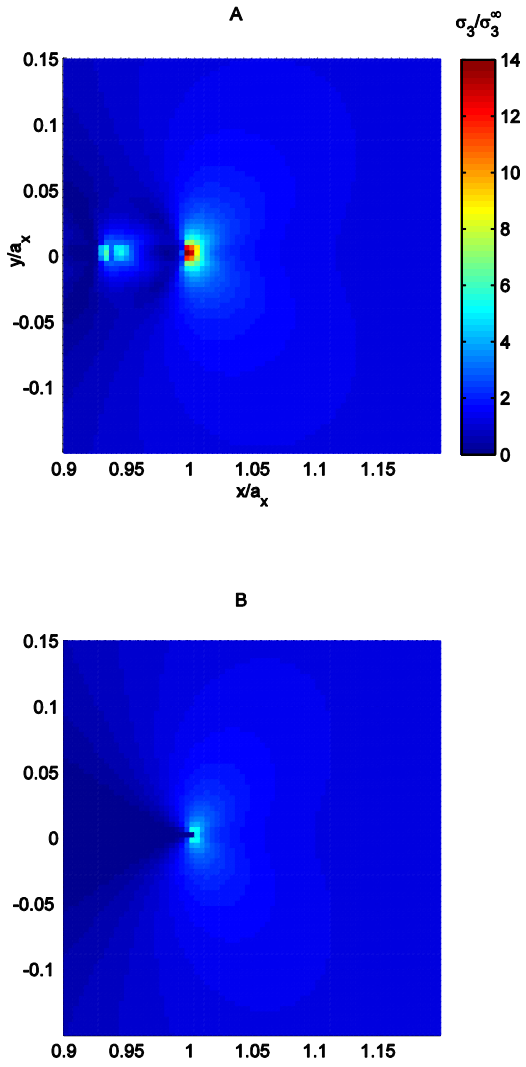

Figure 5 Normalized maximum tensile stress by BEM (**A**) and by Eshelby's solution (**B**) under pure normal stress σ_{zz}^{∞} plotted about the tip at ω=0 on *x*-*o*-*z* plane.

Also, we compare the near-tip stress distributions on the polar coordinates (r,β) at longitude ω=0 and $\pi/2$ in Figure 6.

BEM has a higher order stress concentration than Eshelby's solution as $r\rightarrow 0$.

Both BEM and Eshelby's solution produce near-tip stress that has a *bi-modal* distribution in β for an given distance-to-tip r. The BEM result has some subtle changes at high β angle corresponding to the non-zero scatters on the fracture faces (see Figure 5**A**).

The stress magnitude is higher at ω=π/2 (x=0, y=a_y) than at ω=0 (x=a_x, y=0). Remember we have axial-ratio a_y/a_x<1. This means that the fracture is likely to evolve into a circular shape by growing faster in y directions than in x directions as $a_y \to a_x$, see later sections.

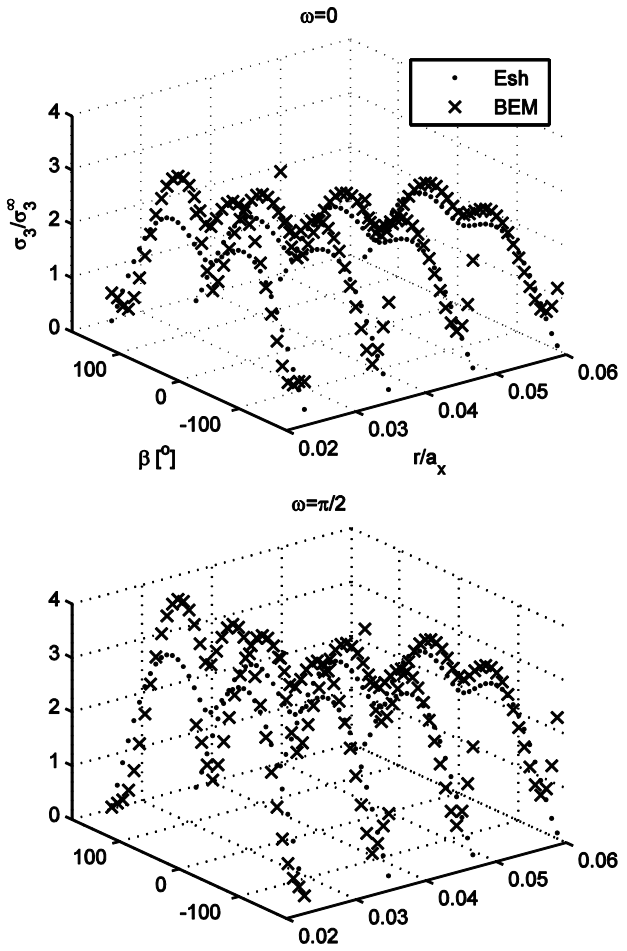

Figure 6 Under uniaxial remote tension σ_{xx}, normalized maximum tensile stress as a function of near tip polar coordinate (r, β) at longitude angle ω=0, π/2.

2.2 Mode I II near-tip stress comparisons

Previous researches [2, 3, 10] analytically formulated the *kink* θ and *twist* φ angles resulting from mode I II and mode I III loadings respective. The limitation was that the fracture tip-line has to be straight (1D). Both BEM and Eshelby's solution overcome this limitation, which enables one to investigate how the tip-line curvature would affect the kink and twist angels.

To have mode I II shear, we rotate the remote stress σ_{zz}^∞ around y-axis by angle η. At longitude ω=0 the fracture tip is under mode I II (see Figure 3).

Similar to Figure 4, we compare the maximum tensile stress by BEM and Eshelby's solution on x-o-z plane, given in Figure 7. Again, the stress distributions by BEM and Eshelby's solution agree well. Compared to Figure 4, the tensile stress kinks by a negative angle at x=a_x, y=0 (ω=0). In later sections we show how this near-tip stress will guide the fracture tip to propagate off-plane.

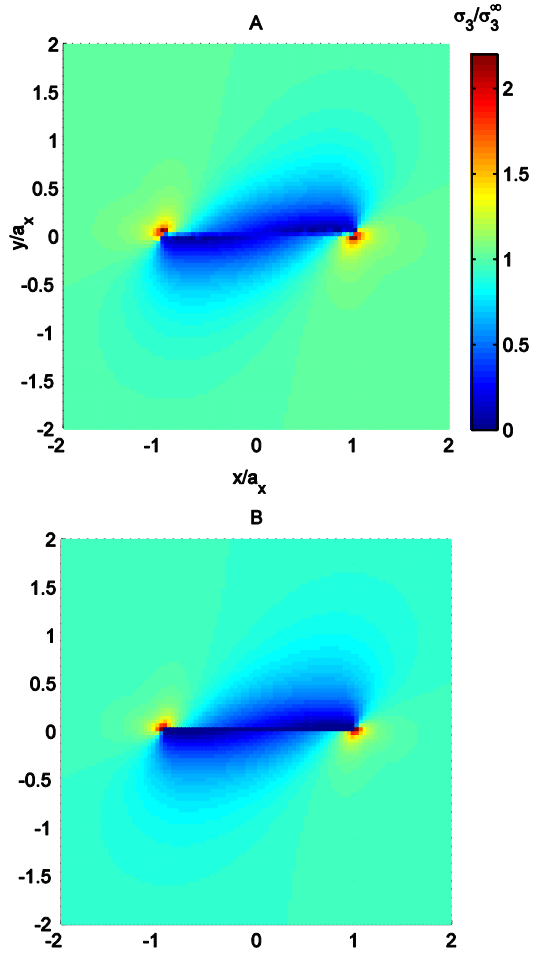

Figure 7 Normalized maximum tensile stress by BEM (**A**) and by Eshelby's solution (**B**) under pure shear stress σ_{xz}^∞ (η=45°) plotted on x-o-z plane.

In Figure 8, we zoom in about the tip at ω=0 to compare the near-tip stresses.

Discrepancy in both magnitude and distribution is noticeable, similar to Figure 5. Despite this, the results by the two models match well.

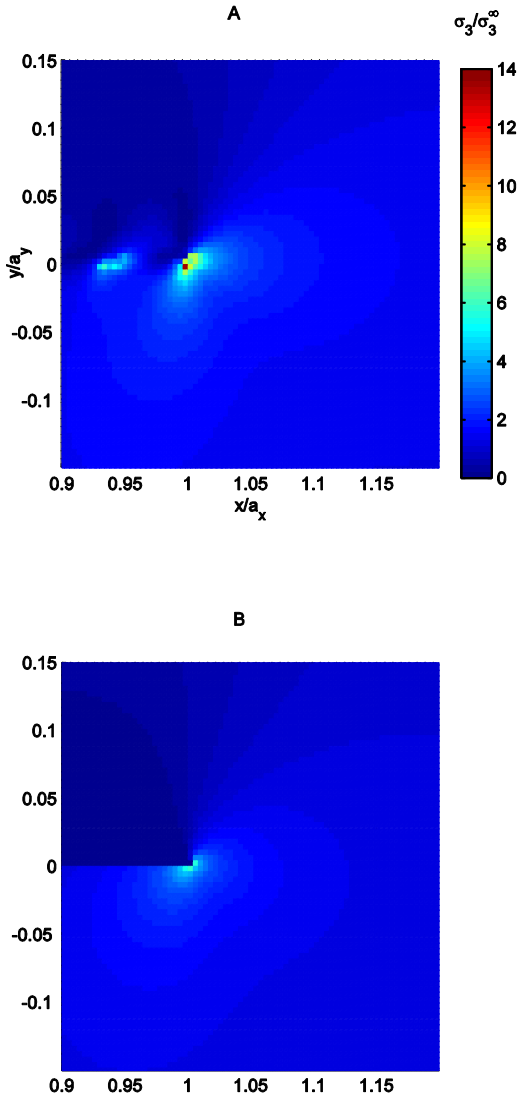

Figure 8 Normalized maximum tensile stress by BEM (**A**) and by Eshelby's solution (**B**) under pure shear stress σ_{xz}^{∞}, (η=45^o) plotted about the tip at ω=0 on *x*-*o*-*z* plane.

Similarly to Figure 6, we compare the stress on the polar coordinates (r,β), given in Figure 9.

Compared to Figure 6, at ω=0 the stress is not symmetric in β and this asymmetry leads to the kink. The *bi-modal* distribution shifts in the negative β direction, which is consistent with Figure 9. At ω=π/2, no shift (kink) occurs since the tip is under mode I III.

Both stress magnitudes are less than in Figure 6. This suggests that the fracture is less likely to grow or will grow slower under the rotated remote stress.

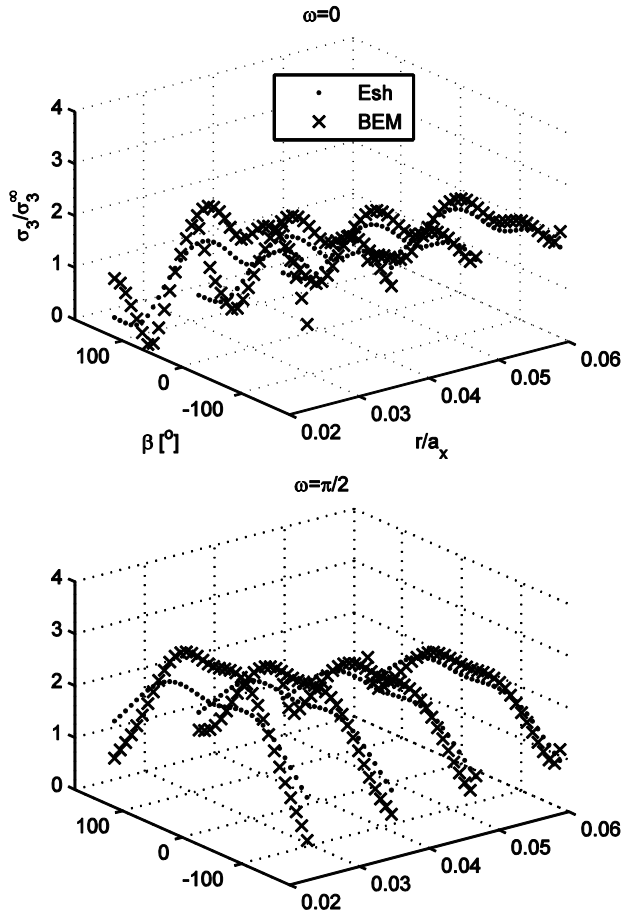

Figure 9 When rotate the uni-axial tensile stress around *y*-axis for η=45^o, normalized maximum tensile stress as a function of near tip polar coordinate (r, β) at longitude angle ω=0, π/2.

Also in Figure 10, we plot the kink angle θ as a function of the axial-ratio a_y/a_x for different stress rotation angle η for ω=0.

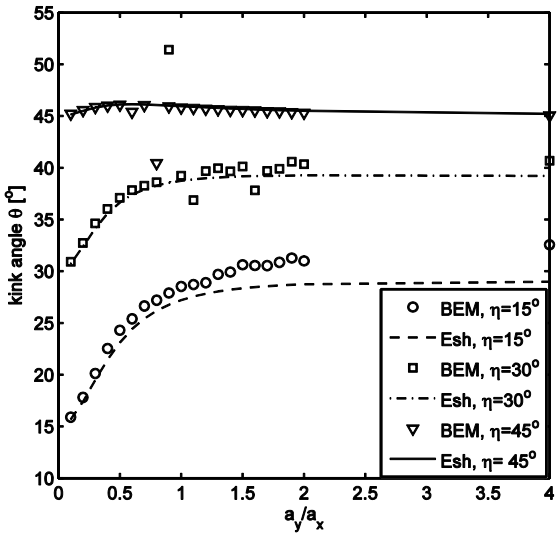

Figure 10 Kink angel θ at longitude ω=0 as a function of axial-ratio a_y/a_x for different stress rotation angle η.

BEM and Eshelby's solution agree well. When $a_y/a_x>1$ and $\eta<45^o$, BEM overshoots Eshelby's solution slightly. The numerical errors of BEM causes some fluctuations while Eshelby's solution always produces smooth curves.

When the stress rotation angel $\eta<45^o$, the kink angle θ increases with a_y/a_x, i.e. a blade shaped tip-line has larger kink angel than that of a finger shaped tip-line.

When $a_y/a_x<<1$ (at the end of a needle shaped fracture) the kink angel is equal to the stress rotation angle, $\theta=\eta$. This suggests that if a fracture is too narrow, it can hardly affect the areas near the end of the *needle* tip in terms of kink angle. In those areas the stresses simply follow the remote stress.

2.1 Mode I III near-tip stress comparisons

In the forgoing example the fracture tip is in mode I III at $\omega=\pi/2$ ($x=0$, $y=a_y$). However the twist angle φ cannot be demonstrated by the lower plot in Figure 9. Nevertheless we make a plot analogous to Figure 10, by rotating the uniaxial tension σ_{zz}^{∞} around the x-axis (see Figure 3)**,** for the same angle η and observe the twist angle φ at $\omega=0$ as a function of axial-ratio a_y/a_x. The BEM and Eshelby's solution result comparisons are given in Figure 11.

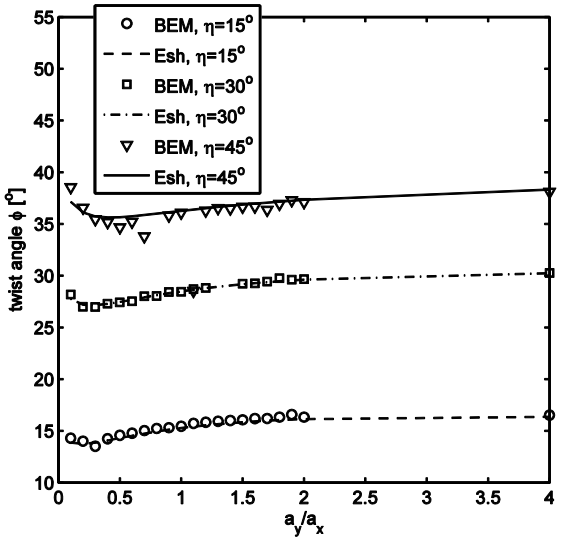

Figure 11 Twist angel φ at $\omega=0$ as functions of axial-ratio a_y/a_x for different x-axis rotation angle η.

The BEM and Eshelby's solution again agree well except for some fluctuations caused by the numerical errors of BEM. The twist angel φ varies somewhat with the axial-ratio a_y/a_x but less than the kink angle (Figure 10). For large stress rotation angles, e.g. $\eta>30^o$, the twist angle under shoots the rotation angle, $\varphi<\eta$. For small rotation angles, e.g. $\eta<15^o$, the twist angle over shoots the rotation angle, $\varphi>\eta$. Similarly to Figure 10, when $a_y/a_x<<1$, the twist angle is equal to the stress rotation angle, $\varphi=\eta$.

3. PROPAGATION MODELING WITH BEM

The stress comparisons in the forgoing section suggest that the BEM can precisely determine the near-tip stress in terms of both magnitude and orientation.

Eshelby's solution as mentioned has a limitation that the fracture has to be ellipsoidal. When the fracture grows into arbitrary geometries, Eshelby's solution will not apply. For this reason we discuss the fracture propagation modeling only in the context of BEM.

We assume a linear relation between the near-tip maximum tensile stress and the fracture tip advancing pace, e.g. from n to $n+1$ in Figure 12.

For the i^{th} edge element on the tip-line, we calculate a propagation vector v_i whose length is proportional to the local maximum tensile stress σ_3 and direction is determined by the kink angle θ and twist angle φ. As demonstrated in Figure 12, we place the origin of the vectors v_i at the center of each associated edge element. By connecting the end of each vector with adjacent two nodes on the associated edge element, a set of new triangular element is created. By connecting the ends of neighboring vectors, a complete ring of new edge elements is then created. This mesh growing method is adopted from [12].

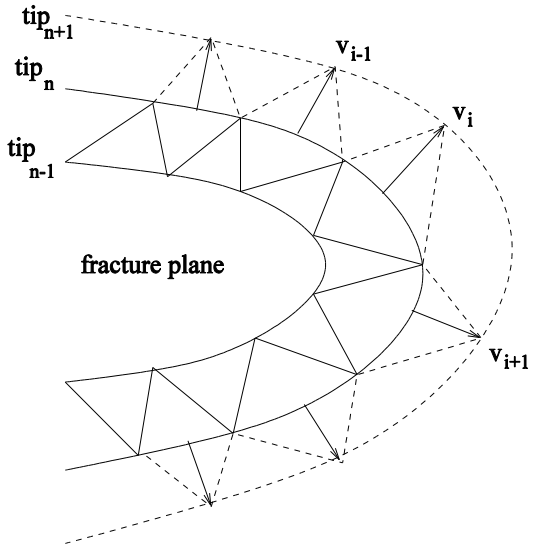

Figure 12 new fracture tip-line formed by alignment of the propagation vector (v_i;) ends; new elements belt formed by connecting the boundary nodes and the propagation vector ends.

3.1. Mode I propagation

We set the elliptical fracture in x-o-y plane with $a_y/a_x=0.5$ and apply uniaxial remote stress $\sigma_{zz}^{\infty}>0$, such that the fracture is in pure mode I.

Figure 13 shows the mesh evolution up to 10 steps. We scale the step length to the maximum near-tip tensile stress normalized by its average value, $\sigma_3/\ \sigma_3^{avg}$, instead of by the remote tensile stress, $\sigma_3/\ \sigma_3^{\infty}$. In this way we can prevent the fracture from growing faster each step, so the element size is not enlarged. This means however the fracture growth is somehow pictured in a *slowing down* time sequence, which allows us to observe the detailed geometry of the evolutionary path.

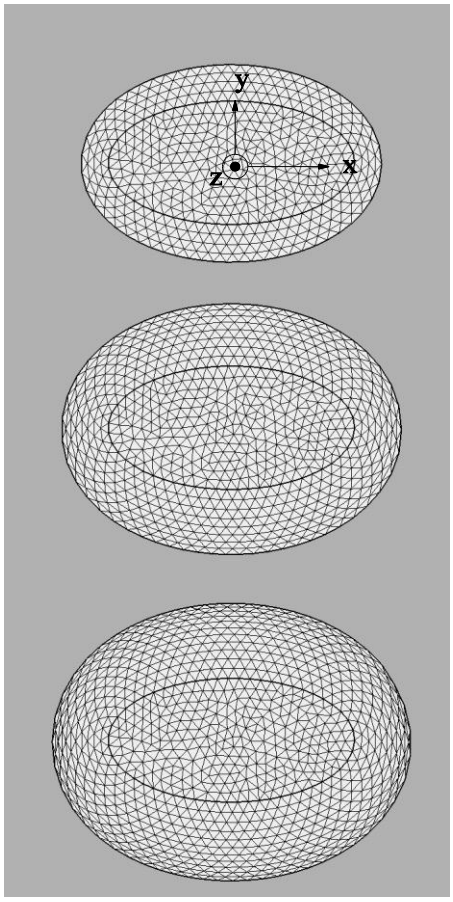

Figure 13 mode I fracture mesh growth with step lengths scaled to the near-tip tensile stress normalized by average tensile stress alone the tip-line.

The elliptical fracture develops into a more circular shape. This is because the near-tip tensile stress is grater at the ends of the short axis than at the ends of the long axis, e.g. $\sigma_{3|\omega=\pi/2} > \sigma_{3|\omega=0}$ in Figure 6.

The fracture is confined within *x-o-y* plane with some tiny fluctuations , $\Delta z/a_x<0.0132$, due to numerical error.

3.2. Mode I II propagation

To have the elliptical fracture in mixed mode, we rotate the uniaxial stress σ_{zz}^{∞} around the *y*-axis by angle η. At the ends of a_x (ω=0,π) the fracture tip is in mode I II, while at the ends of a_y (ω=π/2, 3π/4) the tip is in mode I III.

We take only the kink angle θ into account in calculating the propagation vector v_i and keep the tip-line integrity during mesh evolution, i.e. no segmentation is allowed. The mesh evolution is shown in Figure 14

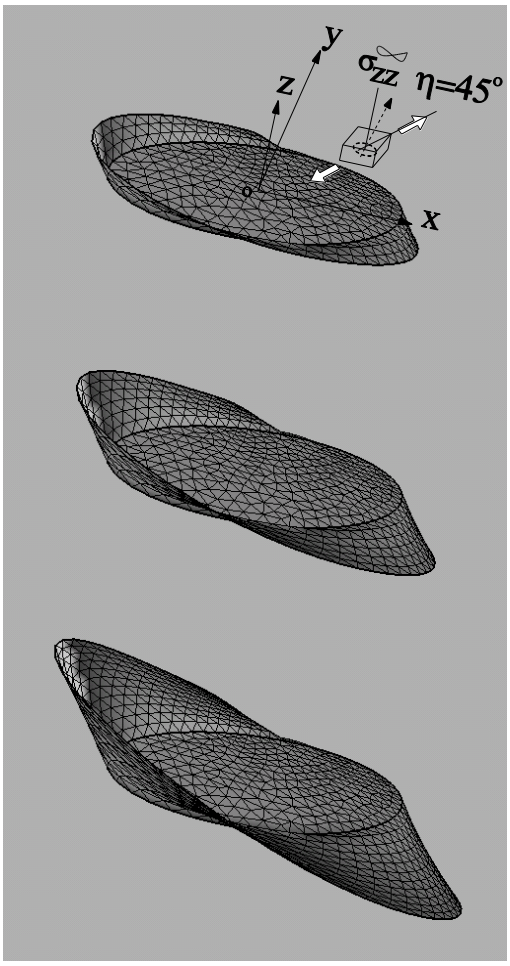

Figure 14 Rotated tensile stress η=45°, mesh evolution when only mod II (kink motion) is considered.

Similar to [12], the tip sections at ω=0,π kink away from *x-o-y* plane to accommodate the rotated stress while at ω=π/2, 3π/4 the tip sections almost stay in the *x-o-y* plane.

3.3. Mode I II III propagation

To model the mode III motion, *twist* and *segmentation*, some care must be taken. We first decide the segment lengths. Within a segment we adjust the kink angel θ of each propagation vector to achieve an effective twist angle φ. The neighboring vectors that are severed by segmentation will not be connected when forming the ring of new edge elements. In this way the tip-line will develop into a twisted and segmented (echelon) shape.

After the desirable twist angle is achieved by each segment, the fracture then propagates without the mode III effect except the gaps between different segment will not be bridged.

The mesh evolution for the same model set-up as in the forgoing example is shown in Figure 15.

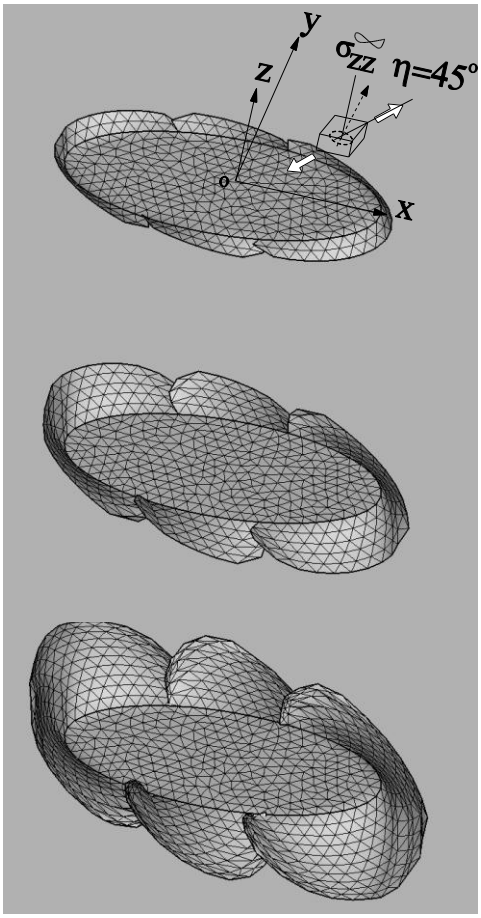

Figure 15 Under rotated tensile stress η=45^o, mesh evolution when mod II (kink) and mode III (twist and segmentation) are considered.

The result looks very different compared to the mode I II example even though the mode III effect only applies to a number of initial steps.

One noticeable feature of such propagation is that the growth at the segment joins are constricted by the segment interactions. Because of this the tip-line extensions are curved, which makes the segments have *petal* shaped geometries that are not depicted in Figure 1B.

4. CONCLUSION AND DISCUSSION

The BEM enables one to calculate a fracture's near-tip stress field precisely. The results are consistent with the analytical Eshelby's solution for elliptical fractures.

The numerical scheme can effectively model mixed mode fracture propagation by running BEM and a propagation criterion in a loop.

The model is capable of capturing both mode II (kink) and mode III (twist) off-plane features. The results suggest that mode III effect has great impact on the resulting fracture shapes.

To model the tip segmentation for different materials, e.g rock, we need to specify a typical segment length which could be dependent on the loading stress, initial fracture shape and material properties. Experimental work is required to characterize the segmentation in each special case.

REFERENCES

1. Erdogan, V.F. and G.C. Sih, *On the crack extension in plates under plane loading and transverse shear.* Trans ASME J Bas Eng, 1963. **85D**(519): p. 519.
2. Thomas, A.L. and D.D. Pollard, *The geometry of echelon fractures in rock: implications from laboratory and numerical experiments.* Journal of Structural Geology, 1993. **15**(3–5): p. 323-334.
3. Cooke, M.L. and D.D. Pollard, *Fracture propagation paths under mixed mode loading within rectangular blocks of polymethyl methacrylate.* J. Geophys. Res., 1996. **101**(B2): p. 3387-3400.
4. Mutlu, O. and D.D. Pollard, *On the patterns of wing cracks along an outcrop scale flaw: A numerical modeling approach using complementarity.* J. Geophys. Res., 2008. **113**(B6): p. B06403.
5. Pons, A.J. and A. Karma, *Helical crack-front instability in mixed-mode fracture.* Nature, 2010. **464**(7285): p. 85-89.
6. Cottrell, B. and J.R. Rice, *Curved or kinked cracks.* Int. J. Fract., 1980. **16**: p. 155.
7. Renshaw, C.E. and D.D. Pollard, *Are large differential stresses required for straight fracture propagation paths?* Journal of Structural Geology, 1994. **16**(6): p. 817-822.
8. Willemse, E.J.M. and D.D. Pollard, *On the orientation and patterns of wing cracks and solution surfaces at the tips of a sliding flaw or fault.* J. Geophys. Res., 1998. **103**(B2): p. 2427-2438.
9. Crouch, S.L. and A. Starfield, *Boundary Element Methods In Solid Mechanics : with Applications In Rock Mechanics and Geological Engineering.* London: Allen & Unwin, 1983.
10. Olson, J.E. and D.D. Pollard, *The initiation and growth of en échelon veins.* Journal of Structural Geology, 1991. **13**(5): p. 595-608.
11. POLLARD, D.D., P. SEGALL, and P.T. DELANEY, *Formation and interpretation of dilatant echelon cracks.* Geological Society of America Bulletin, 1982. **93**(12): p. 1291-1303.
12. Forth, S.C., W.D. Keat, and L.H. Favrow, *Experimental and computational investigation of three-dimensional mixed-mode fatigue.* Fatigue & Fracture of Engineering Materials & Structures, 2002. **25**(1): p. 3-15.
13. Thomas, A., *POLY3D: A Three-Dimensional, Polygonal Element, Displacement Discontinuity Boundary Element Computer Program with Applications to Fractures, Faults, and Cavities in*

the {E}arth's Crust. 1993, Department of Geology, Stanford University. p. 69.
14. Maerten, F., L. Maerten, and M. Cooke, *Solving 3D boundary element problems using constrained iterative approach.* Computational Geosciences, 2010. **14**(4): p. 551-564.
15. Comninou, M. and J. Dundurs, *The angular dislocation in a half space.* Journal of Elasticity, 1975. **5**(3): p. 203-216.
16. Jeyakumaran, M., J.W. Rudnicki, and L.M. Keer, *Modeling slip zones with triangular dislocation elements.* Bulletin of the Seismological Society of America, 1992. **82**(5): p. 2153-2169.
17. Eshelby, J.D., *The Determination of the Elastic Field of an Ellipsoidal Inclusion, and Related Problems.* Proceedings of the Royal Society of London. Series A, Mathematical and Physical Sciences, 1957. **241**(1226): p. 376-396.
18. Eshelby, J.D., *The Elastic Field Outside an Ellipsoidal Inclusion.* Proceedings of the Royal Society of London. Series A, Mathematical and Physical Sciences, 1959. **252**(1271): p. 561-569.
19. Eshelby, J.D., *Elastic inclusions and inhomogeneities.* Progress in solid mechanics, 1961. **2**: p. 89-140.
20. Mura, T., *Micromechanics of defects in solids*. Mechanics of elastic and inelastic solids. 1987: Kluwer Academic Pub.
21. Meng, C., W. Heltsley, and D.D. Pollard, *Evaluation of the Eshelby solution for the ellipsoidal inclusion and heterogeneity.* Computers & Geosciences, 2011(0).
22. Maugis, D., *Adhesion of spheres: The JKR-DMT transition using a dugdale model.* Journal of Colloid and Interface Science, 1992. **150**(1): p. 243-269.